International Journal of Thermal Sciences 145 (2019) 106001

Contents lists available at ScienceDirect

International Journal of Thermal Sciences

journal homepage: www.elsevier.com/locate/ijts

Impacts of the flexibility of a thin heater plate on the natural convection heat transfer

Seyed Mohsen Hashem Zadeh[a], S.A.M. Mehryan[b], E. Izadpanahi[c], Mohammad Ghalambaz[d,e,*]

[a] Department of Mechanical Engineering, Shahid Chamran University of Ahvaz, Ahvaz, Iran
[b] Young Researchers and Elite Club, Yasooj Branch, Islamic Azad University, Yasooj, Iran
[c] Department of Mechanical and Materials Engineering, Florida International University, Miami, FL 33174, United States
[d] Department for Management of Science and Technology Development, Ton Duc Thang University, Ho Chi Minh City, Vietnam
[e] Faculty of Applied Sciences, Ton Duc Thang University, Ho Chi Minh City, Vietnam

ARTICLE INFO

Keywords:
FSI
Flexibile thin plate
Natural convection
Enclosure

ABSTRACT

Fluid-solid interaction study is conducted to investigate the effects of the flexibility of thin plate on the natural convection inside an enclosure. The plate is assumed to be at a higher temperature while the side walls are at a colder temperature and the top and bottom walls are insulated. The inclination angle of the plate is considered constant; however, other parameters such as the height and length of the plate, the elasticity modulus, Rayleigh number, and Prandtl number are varied, and their effects are studied. The grid independence study is presented, and the results are verified against available data in the literature. The effects of the plate flexibility on the flow and heat transfer are addressed. It is found that the Nusselt number and the strength of the flow decrease as the plate become more flexible. Additionally, as the plate moves toward the bottom of the cavity, the Nusselt number increase but the strength of the vortices decreases. Finally, the effects of flexibility is found to be considerable and it completely depends on the flow regime and other parameters.

1. Introduction

Manipulation of the design parameters is the key component in the evolution of any design. Numerous ways have been proposed with the purpose of heat transfer enhancement in thermal systems. Likewise, forced and natural convections [1–7], which have a variety of applications such as electronic packaging, solar collectors, thermofluid and energy storage systems, is comprehensively investigated throughout literature. However, there are limited studies that investigate the effects of fluid-solid interaction on natural convection inside enclosures [8–12], which it has a significant effect on the behavior of the flow domain as well as the heat transfer rate. This is due to the complexity and time-consuming nature of these problems as well as hardware limitations. Nowadays such numerical analysis becomes more convenient.

Some studies considered the cavity wall to be flexible [8,9], while others investigated the cavity with a flexible plate or membrane inside the cavity [10–13]. There are many industrial applications for both of these configurations. For instance, enclosures with electronic boards inside or enclosures with multiple electronic units, which are separated into partitions utilizing thermal conductive plates, are examples of the application of these configurations [9]. Other examples can be observed in batteries or chemical reactors where two different chemical fluid should be separated [10].

When the cavity contains a flexible wall, it was reported that the flexibility of the flexible wall has a significant influence on the heat transfer rate inside the enclosure [8,9]. The comparison between the average Nusselt number of rigid wall and a flexible wall was presented. In the case of mix convection [8], it was reported that the maximum difference between the Nusselt number of a cavity with a rigid and flexible bottom wall is 9.4%, which decreases as Reynolds number increases. On the other hand, in the case of natural convection [9], the maximum difference in Nusselt number of a cavity with rigid and flexible side wall was reported equal to 13.6%. It was also found that the difference in Nusselt number increases with the Rayleigh number.

Additionally, the results of natural convection inside cavities containing flexible partitions [10] or flexible fin [11] showed that the heat transfer increases as flexibility increases. It is mentioned that [10], this is since the flexibility of the structure increases the shape of the membrane changes in accordance to the flow pattern, which causes a

* Corresponding author. Department for Management of Science and Technology Development, Ton Duc Thang University, Ho Chi Minh City, Vietnam.
E-mail addresses: mohsen.hashemzadeh@gmail.com (S.M. Hashem Zadeh), alal171366244@gmail.com (S.A.M. Mehryan), eizad001@fiu.edu (E. Izadpanahi), mohammad.ghalambaz@tdtu.edu.vn (M. Ghalambaz).

https://doi.org/10.1016/j.ijthermalsci.2019.106001
Received 14 August 2018; Received in revised form 9 April 2019; Accepted 25 June 2019
Available online 05 July 2019
1290-0729/ © 2019 Elsevier Masson SAS. All rights reserved.

Nomenclature

$\boldsymbol{d}_s$	vector of displacement
E	Young's modulus in dimensional form
E_τ	elasticity modulus in non-dimensional form
f	frequency
$\boldsymbol{F}_v$	vector of body force
$\boldsymbol{g}$	vector of gravity acceleration
L	size of cavity
P	fluid pressure
Pr	Prandtl number
Ra	thermal Rayleigh number
t	dimensional time
T	temperature
$\boldsymbol{u}$	vector of velocity
$\boldsymbol{w}$	velocity vector of the moving grid
x	Cartesian coordinate in x direction
y	Cartesian coordinate in y direction

Greek symbols

α	thermal diffusivity
β	volumetric thermal expansion coefficient
σ	Tensor of stress
τ	non-dimensional time
μ	dynamic viscosity
ν	Poisson's ratio
ρ	density
ρ_R	density ratio of fluid to solid structure

Subscripts

avg	average
c	cold temperature
f	fluid
h	hot temperature
p	membrane partition
s	flexible plate

Superscripts

tr	transpose of matrix
*	indicates the dimensional parameter

significant increase in the heat transfer. On the contrary, the resistance to the flow pattern increases and causes a reduction in the heat transfer as the partition becomes more rigid.

The natural convection of a heated plate inside an enclosure is a very well-known problem [14–18] with different industrial applications. Several attempts have been made to investigate this problem [14–18]. Different geometry changes have been proposed to increase the heat transfer from the plate. Some investigated horizontal positioning of the plate [16], while others studied vertical and horizontal [14,15,17]. Additionally, Zhang et al. [18] investigated the heated plate with a different angle of inclination. In all of these studies, it was found that the change in geometry significantly affects the heat transfer rate from the heated plate. For example, Hakeem et al. [14] found that the enhancement in heat transfer is more significant when the plate is in the vertical position compared to the horizontal one for the case of isothermal boundary condition, while for the case of isoflux boundary, the heat transfer rate of a horizontally mounted plate is higher.

In Ref. [11] there was a fin which was subject to a prescribed tip movement. However, the structure of the fin was subject to interaction with the natural convection flow. Indeed [11], was a mixed convection heat transfer flow in a cavity. In the present study, the fin is passive, and the deflection of the fins is solely due to the interaction with the natural convection flow in the cavity.

In the studies as mentioned earlier, the fluid-solid interaction between the heated plate and the flow inside the enclosure was not taken into account. Since it was mentioned that the flexibility of the part affects the heat transfer significantly [8–12], in this study, these effects are implemented to fully investigate the heat transfer problem from heated plate inside a cavity. Authors aim to comprehensively investigate this problem due to the great importance and application of it. After the grid dependency study, comparisons are made with the results available in the literature to verify the current method. Then, the results for a large range of Rayleigh number, elasticity modulus, the Prandtl number and the height of the plate from the origin are presented.

2. Definition and mathematics of the problem

Fig. 1 illustrates the schematic view of the investigated cavity. The origin of the coordinate system is defined at the center of the cavity. The width and height of the cavity considered to be equal, $L^* = W^*$. The left and right bounds are at the temperature of T_c^*, whereas the top and bottom walls are thermally insulated. A hot flexible thin plate with the temperature of T_h^* is placed horizontally inside the cavity. The cavity bounds are stationary and no-slip condition is taken into account on them. The flexible thin plate of thickness t_p^* is isotropic and uniform. Boundaries of the enclosure and flexible thin plate are impervious. The variations of the fluid density are approximated by employing Boussinesq's approximation. The gravity force is imposed on the cavity in the vertical direction. The body forces applied to the plate includes the weight of the plate and the buoyancy force.

The governing equations including the mass, momentum and energy conversation ones considering the mentioned assumptions for an incompressible, laminar and Newtonian fluid, and the arbitrary Lagrangian-Eulerian (ALE) technique, are [19].

Continuity equation:

$$\nabla^* \cdot \mathbf{u}^* = 0 \tag{1}$$

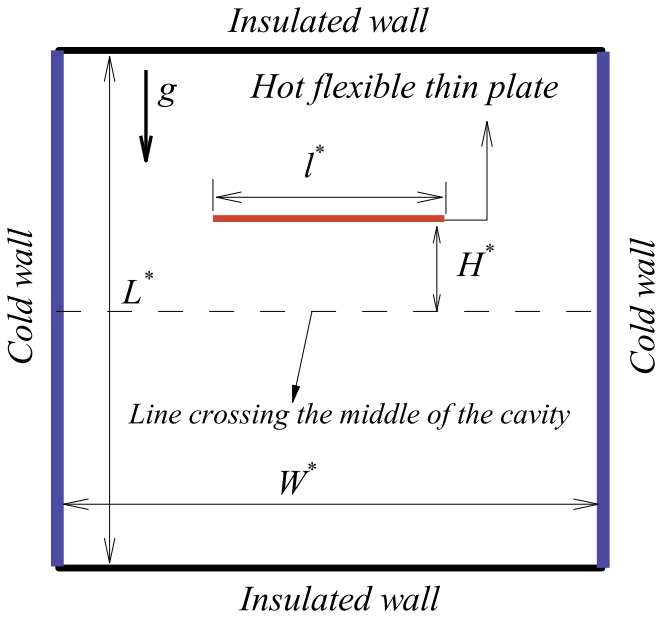

Fig. 1. A schematic of the problem.

Momentum equations:

$$\frac{\partial \mathbf{u}^*}{\partial t} + (\mathbf{u}^* - \mathbf{w}^*)\cdot\nabla^*\mathbf{u}^* = -\frac{1}{\rho_f}\nabla^* P^* + \nu_f \nabla^{*2}\mathbf{u}^* + \beta \mathbf{g}(T^* - T_c^*) \tag{2}$$

Energy equation:

$$\frac{\partial T^*}{\partial t} + (\mathbf{u}^* - \mathbf{w}^*)\cdot\nabla^* T^* = \alpha_f \nabla^{*2} T^* \tag{3}$$

Moreover, the following nonlinear elastodynamic equation can describe the structural displacement of the flexible plate:

$$\rho_s \frac{d^2 \mathbf{d}_s^*}{dt^2} - \nabla^*\boldsymbol{\sigma}^* = \mathbf{F}_v^* \tag{4}$$

where $\mathbf{u}^* = (u^*, v^*)$ is the velocity vector of fluid, $\mathbf{w}^* = (u_s^*, v_s^*)$ the velocity of moving coordinate system, P^* the pressure of the fluid T^* the temperature of the solid/fluid, $\mathbf{g}$ the gravity acceleration. $\mathbf{d}_s^*$ is the displacement vector of the plate so that $d\mathbf{d}_s^*/dt = \mathbf{w}^*$, $\boldsymbol{\sigma}^*$ the solid stress tensor, $\mathbf{F}_v^*$ the body force applied to the thin plate. ρ is the density and subscripts of f and s refer to the fluid and solid, respectively. ν_f is the kinematic viscosity, α_f thermal diffusivity of the fluid and β the volumetric thermal expansion coefficient of the fluid.

The Neo-Hookean solid model is utilized to represent the stress tensor of Eq. (4).

$$\boldsymbol{\sigma}^* = J^{-1} F S F^{tr} \tag{5}$$

F^{tr} is the transpose of matrix F. S, known as the Piola–Kirchhoff stress tensor, is related to the strain energy density function W_s and the strain ε.

$$F = (I + \nabla^*\mathbf{d}_s^*),\ J = det(F) \text{ and } S = \partial W_s/\partial\varepsilon \tag{6}$$

$$W_s = \frac{1}{2}\mu_l (J^{-1}I_1 - 3) - \mu_l \ln(J) + \frac{1}{2}\lambda(\ln(J))^2 \tag{7}$$

$$\varepsilon = \frac{1}{2}(\nabla^*\mathbf{d}_s^* + \nabla^*\mathbf{d}_s^{*tr} + \nabla^*\mathbf{d}_s^{*tr}\nabla^*\mathbf{d}_s^*) \tag{8}$$

where λ and μ_l are known as Lame's first and second parameters, respectively, and are achieved by the following relations:

$$\mu_l = E/(2(1+\nu)) \tag{9}$$

$$\lambda = E\nu/((1+\nu)(1-2\nu)) \tag{10}$$

The boundary conditions on the interface boundaries between the fluid and the flexible thin plate, as well as, on the external bounds are

$$T^* = T_h^*, \quad \frac{\partial \mathbf{d}_s^*}{\partial t} = \mathbf{u}^*,\ \boldsymbol{\sigma}^*.\, n = -P^* + \mu_f \nabla^*\mathbf{u}^* \quad \forall\, x^*, y^* \ \exists \begin{cases} y^* = H^*, & -\frac{l^*}{2} \le x^* \le \frac{l^*}{2} \\ y^* = H^* + t_p^*, & -\frac{l^*}{2} \le x^* \le \frac{l^*}{2} \\ x^* = -\frac{l^*}{2}, & -\frac{l^*}{2} \le y^* \le \frac{l^*}{2} \\ x^* = \frac{l^*}{2}, & -\frac{l^*}{2} \le y^* \le \frac{l^*}{2} \end{cases} \tag{11-a}$$

$$T^* = T_c^*, \quad u^* = v^* = 0 \quad \forall\ x^*,\ y^*\ \exists \begin{cases} x^* = 0\ , & 0 \le y^* \le L^* \\ x^* = L^*, & 0 \le y^* \le L^* \end{cases} \tag{11-b}$$

$$\frac{\partial T^*}{\partial y^*} = 0,\ u^* = v^* = 0 \quad \forall\ x^*, y^*\ \exists \begin{cases} y^* = 0\ , & 0 \le x^* \le L^* \\ y^* = L^*, & 0 \le x^* \le L^* \end{cases} \tag{11-c}$$

The dimensional governing equations (1)–(4) can be converted into non-dimensional equations using the following dimensionless parameters:

$$\mathbf{d}_s = \frac{\mathbf{d}_s^*}{L^*},\ \boldsymbol{\sigma} = \frac{\boldsymbol{\sigma}^*}{E},\ \tau = \frac{t\alpha_f}{L^{*2}},\ (x, y, H) = \frac{(x^*, y^*, H^*)}{L^*}$$
$$\mathbf{u} = \frac{\mathbf{u}^* L^*}{\alpha_f},\ \mathbf{w} = \frac{\mathbf{w}^* L^*}{\alpha_f},\ P = \frac{P^* L^{*2}}{\rho_f \alpha_f^2},\ T = \frac{T^* - T_c^*}{T_h^* - T_c^*}$$
$$\nabla^* = \frac{\nabla}{1/L^*},\ t_p = \frac{t_p^*}{L^*} \tag{12}$$

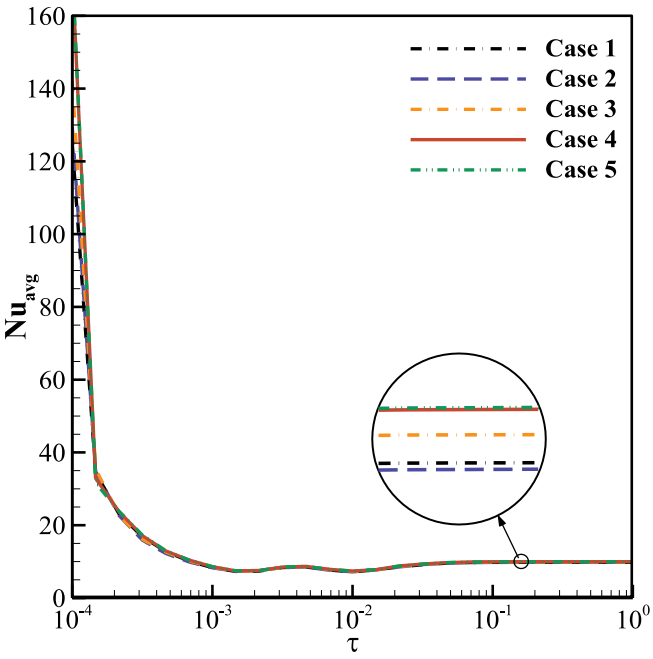

Fig. 2. Time variation of average Nusselt numbers for various numerical grid.

Table 1
The required time and memory for grid size independency.

Cases	No. of elements	Run time	Memory
Case 1	5315	13 min, 17 s	1.56 GB
Case 2	7897	3 min, 49 s	1.58 GB
Case 3	10529	4 min, 44 s	1.64 GB
Case 4	26482	11 min, 12 s	2.04 GB
Case 5	34766	16 min, 25 s	2.11 GB

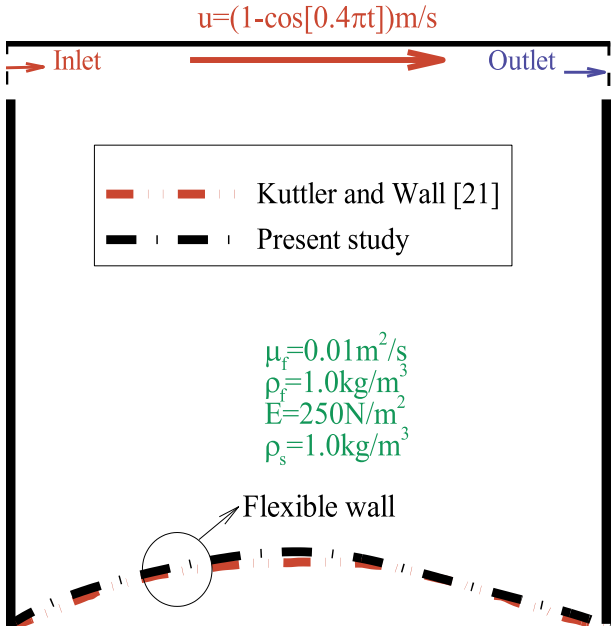

Fig. 3. The evaluation of the current study results and the results reported by Kuttler and Wall [21].

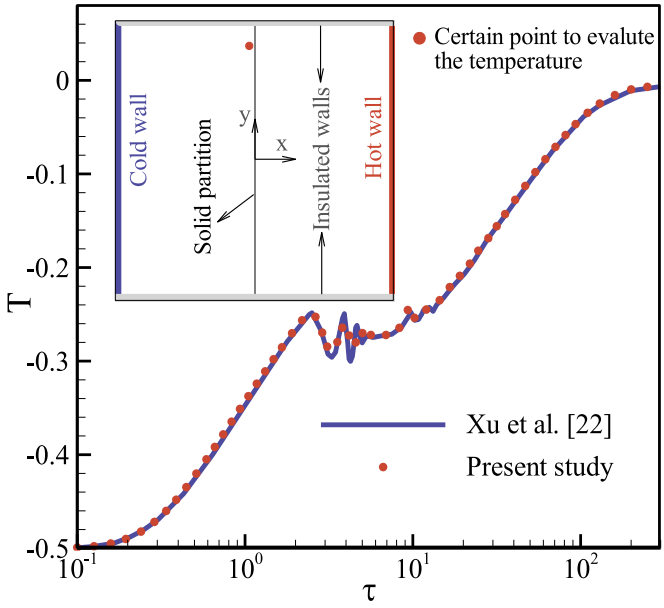

Fig. 4. The values of temperature in typical point of square enclosure of the presents study and work of Xu et al. [22].

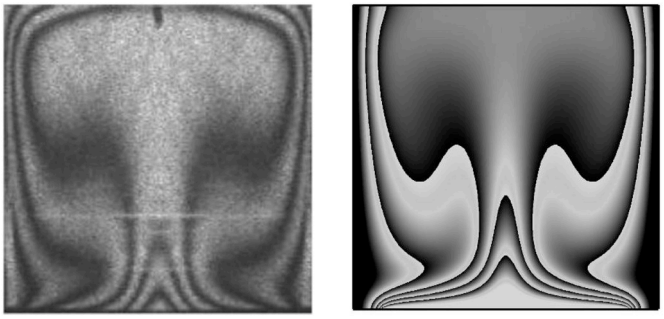

a b

Fig. 5. a: Experimental temperature field presented by Calcagni et al. [23] and b: numerical temperature field obtained in the present study.

In the non-dimensional form, we then have

$$\nabla\cdot\mathbf{u} = 0 \tag{13}$$

$$\frac{\partial \mathbf{u}}{\partial \tau} + (\mathbf{u}-\mathbf{w})\cdot\nabla\mathbf{u} = -\nabla P + Pr\nabla^2\mathbf{u} + PrRaT\mathbf{j} \tag{14}$$

$$\frac{\partial T}{\partial \tau} + (\mathbf{u}-\mathbf{w})\cdot\nabla T = \nabla^2 T \tag{15}$$

$$\frac{1}{\rho_R}\frac{d^2\mathbf{d}_s}{d\tau^2} - E_\tau\nabla\boldsymbol{\sigma} = E_\tau\mathbf{F}_v \tag{16}$$

where

$$Ra = \frac{g\beta(T_h^* - T_c^*)L^{*3}}{\upsilon_f\alpha_f},\ Pr = \frac{\upsilon_f}{\alpha_f},\ E_\tau = \frac{EL^{*2}}{\rho_f\alpha_f^2},\ \mathbf{F}_v = \frac{(\rho_f-\rho_s)L^*\mathbf{g}}{E},\ \rho_R = \frac{\rho_f}{\rho_s} \tag{17}$$

In the present work the buoyancy force applied to the flexible plate is ignored (i.e., $\mathbf{F}_\nu = 0$). The dimensionless boundary conditions are

$$T = 1,\quad \frac{\partial \mathbf{d}_s}{\partial t} = \mathbf{u},\ \boldsymbol{\sigma}\cdot n = -P + Pr\nabla\mathbf{u} \quad \forall\ x,y\ \exists \begin{cases} y = H, & -\frac{l}{2}\le x\le\frac{l}{2} \\ y = H + t_p, & -\frac{l}{2}\le x\le\frac{l}{2} \\ x = -\frac{l}{2}, & -\frac{l}{2}\le y\le\frac{l}{2} \\ x = \frac{l}{2}, & -\frac{l}{2}\le y\le\frac{l}{2} \end{cases} \tag{18-a}$$

$$T = 0,\quad u = v = 0 \quad \forall\ x,y\ \exists \begin{cases} x = 0, & 0\le y\le 1 \\ x = 1, & 0\le y\le 1 \end{cases} \tag{18-b}$$

$$\frac{\partial T}{\partial y} = 0,\quad u = v = 0 \quad \forall\ x,y\ \exists \begin{cases} y = 0, & 0\le x\le 1 \\ y = 1, & 0\le x\le 1 \end{cases} \tag{18-c}$$

In dimensionless coordinate, the initial velocity and pressure of the fluid are equal to zero. Moreover, the initial temperature is 0.5. Local Nusselt number on the plate is used to measure the rate of heat transfer:

$$Nu_{local} = -\left.\frac{\partial T}{\partial n}\right|_{On\ the\ hot\ plate} \tag{19}$$

where n is the normal direction to the surface of the flexible plate. Besides, the average Nusselt number is achieved by integration on the hot plate bounds:

$$Nu_{avg} = \frac{1}{2\,(l + t_{fin})}\int_{Hot\ plate} Nu_{local}\,ds \tag{20}$$

Finally, the stream function ψ is employed in describing the flow pattern:

$$u = \frac{\partial\psi}{\partial y},\quad v = -\frac{\partial\psi}{\partial x} \tag{21}$$

3. Numerical solution and validations

3.1. Grid independence test

The non-dimensional governing equations along with the mentioned boundary conditions are initially converted to the form of the weak solution, then solved by applying the Galerkin finite element method. The Galerkin finite element approach is completely given in Ref. [20] in details. The coupling between the fluid and structure are used using a free deformed mesh technique based on the arbitrary

Table 2
Comparison of average convective Nusselt numbers (on the outer cold wall) and $|\psi_{max}|$ with Saravanan and Sivaraj [17] for l = 0.5 and zero wall emissivity.

	Ra = 10^5		Ra = 10^6		Ra = 10^7	
	Nu_{avg}	$\lvert\psi_{max}\rvert$	Nu_{avg}	$\lvert\psi_{max}\rvert$	Nu_{avg}	$\lvert\psi_{max}\rvert$
Current study	3.2774	7.0928	5.1558	15.471	8.4297	32.6441
Saravanan and Sivaraj [17]	3.3339	7.0358	5.2804	15.5904	8.7997	32.4851
Error (%)	1.69	0.81	2.36	0.77	4.20	0.49

Lagrangian-Eulerian method. The deformation of the solid domain is computed based on the Lagrangian method while the heat and flow equations are solved using the Eulerian method. The moving of the mesh is calculated using the Laplace method following the motion of the solid parts. Indeed, the term **u**-**w** accounts the absolute velocity of the fluid by considering the effect of the moving grid. We tried to solve the governing equations using a Segregated solver iteratively. However, the solution was not stable and failed to converge. Hence, we used the fully coupled method to solve all of the equations, simultaneously. It is worth noting that using fully coupled equations increases the required computational memory, but the solution is stable. An automatic time step scheme with free steps based on the backward Euler method is also

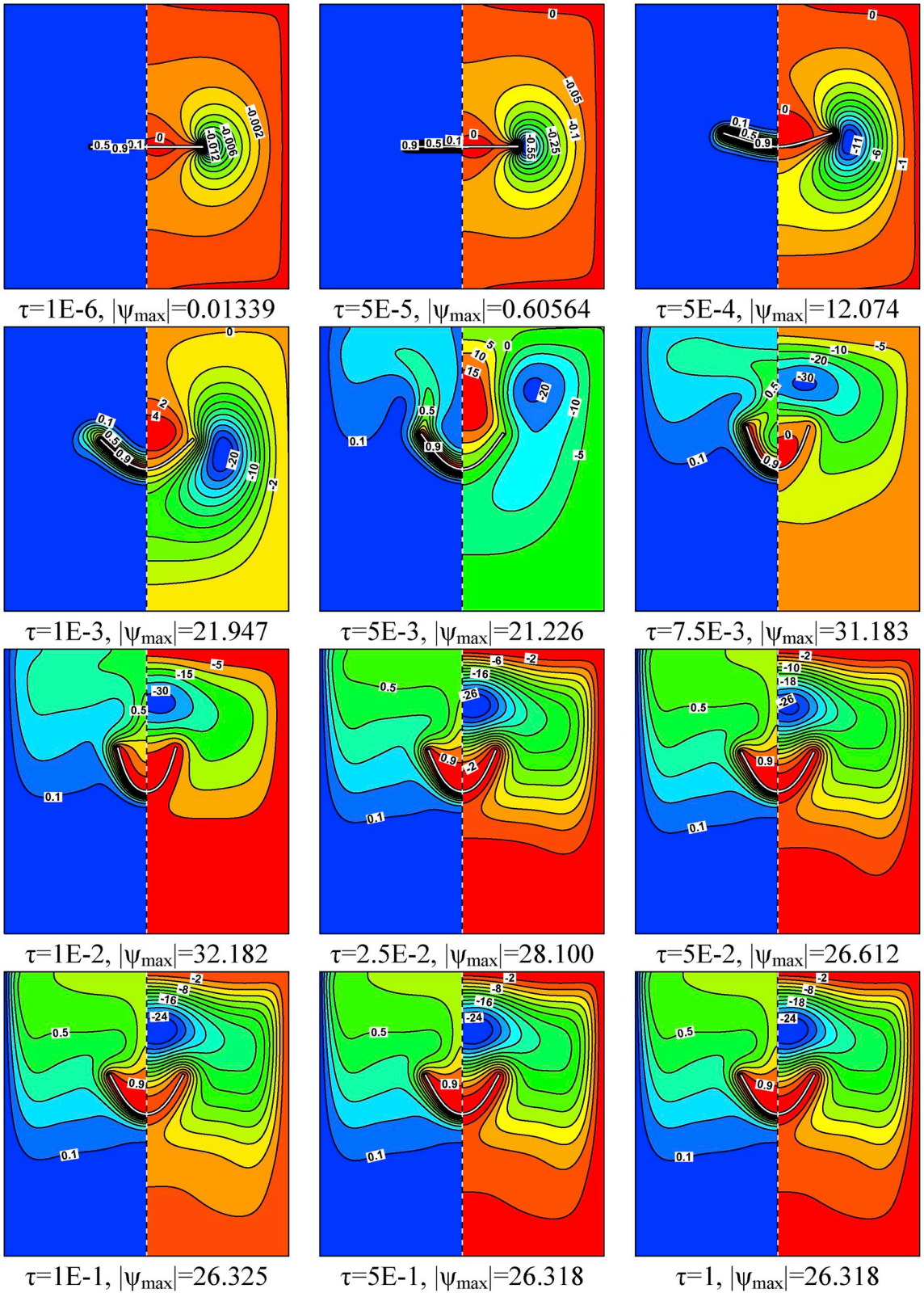

Fig. 6. Time variation of isotherms (left) and streamlines (right) (Ra = 10^6, Pr = 6.2, $E_\tau = 5 \times 10^9$, l = 0.4, H = 0.0).

Table 3
Variation of the $|\psi_{max}|$ and Nu_{avg} (on the hot flexible plate) with non-dimensional time at different values of the elasticity modulus (H = 0.0, Ra = 10^6, Pr = 6.2, l = 0.4).

	E_τ	τ									
		1E-6	1E-5	1E-4	5E-4	1E-3	5E-3	1E-2	5E-2	1E-1	5E-1
$\|\psi_{max}\|$	5×10^9	0.0134	0.1004	1.5082	12.074	21.947	21.226	32.182	26.612	26.325	26.318
	5×10^{10}	0.0131	0.0992	1.3224	4.0309	8.4661	30.995	67.314	46.850	45.664	45.753
	Rigid	0.0044	0.0326	0.3970	3.2171	7.3762	71.789	68.383	49.502	47.385	47.121
Nu_{avg}	5×10^9	435.04	327.81	48.998	27.339	21.260	21.690	14.919	12.042	11.894	11.882
	5×10^{10}	435.04	329.44	49.567	27.259	20.257	17.133	15.084	12.286	12.071	12.071
	Rigid	435.04	355.27	54.645	29.443	21.645	16.181	15.144	12.305	12.082	12.084

utilized to monitor time steps and prevent divergence of the solution.

The grid independence test is of the most important stages of every numerical work so that sometimes ignoring that can cause a drastic deviation from the correct results. In this work, this examination is performed for five grids of different sizes. According to the outcomes illustrated in Fig. 2, although the grid with 10529 elements seems to be accurate enough, the grid with 26842 elements is chosen to achieve the results with the proper accuracy. Table 1 shows the computational time and required memory of the calculations for various grid sizes. The calculations were performed using a computer with 16 GB of Memory, 8 CPU cores each of 2.4 GHz. As shown, for the lowest number of elements, the run time is incredibly high and it decreases dramatically when the elements number reaches to 7879. In fact, higher number of iterations in each time step is required to reach the convergence criteria for the coarse grid of the case 1. Hence, the run time is high. As expected, the required memory rises as the elements number increase.

3.2. Comparisons with others

Another most important stage in a numerical work is verification for confirming the correctness and accuracy of the presented results. Several verifications are performed to achieve this goal. In the first

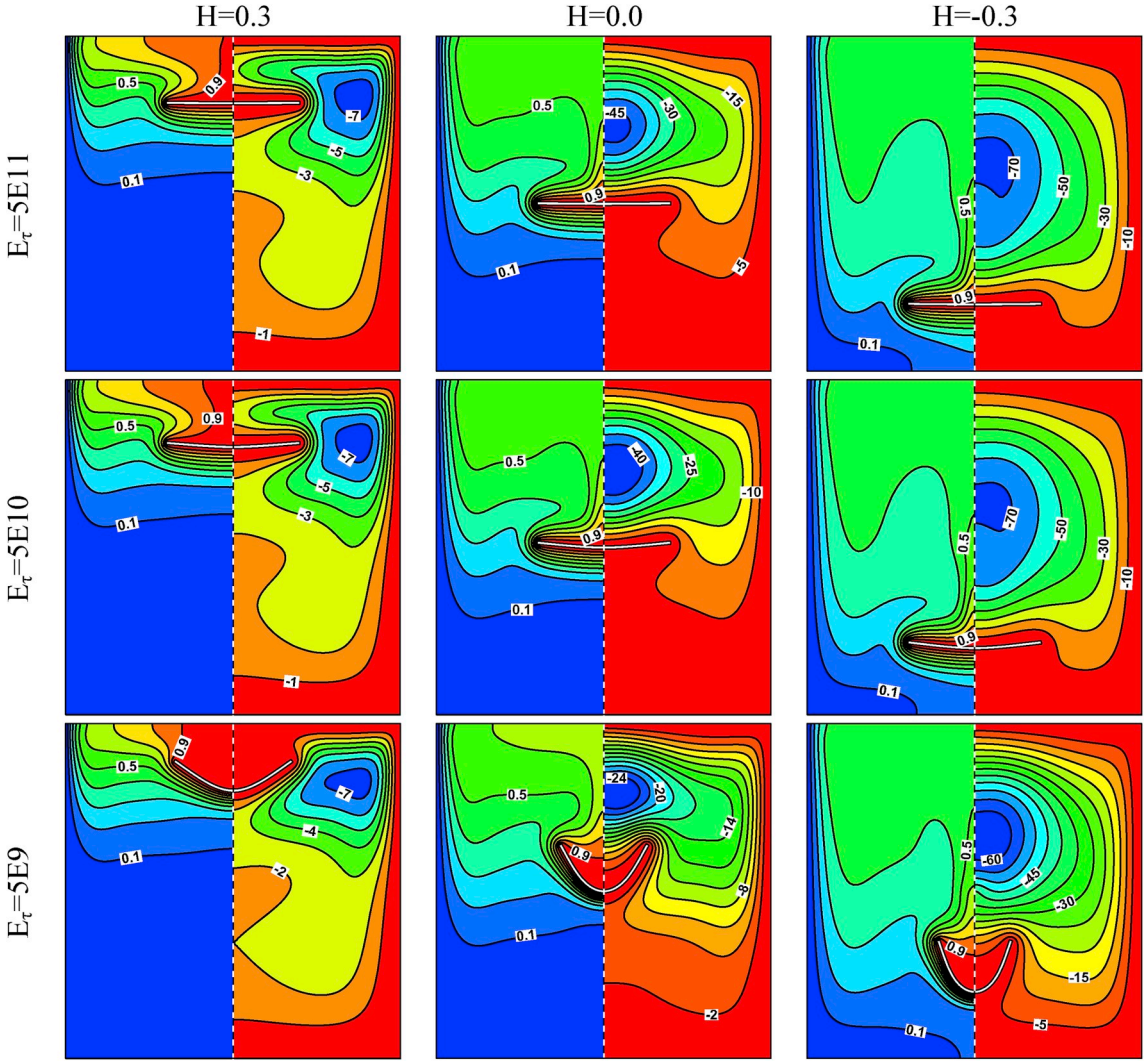

Fig. 7. Effect of Elasticity modulus on the steady state isotherms (left) and Streamlines (right) for different values of H (0.3, 0.0 and −0.3), (Pr = 6.2, Ra = 10^6, l = 0.4).

verification (Fig. 3), the results obtained in the current work and those reported by Ref. [21] are compared to each other. A Lid-driven cavity having a pliable wall was modeled in Ref. [21]. As illustrated, there is excellent compatibility between the results related to the deformability of the bottom walls.

In another verification, the outcomes of the present study and those presented by Xu et al. [22] are compared. As shown in Fig. 4, there exists satisfactory accordance between the results of the current model and the results found by Xu et al. [22]. In addition, the numerical results of the present study are validated by comparing with the experimental results reported by Calcagni et al. [19] as depicted in Fig. 5. It can evidently be seen that the present results are reliable. Eventually, the present results and those reported by Saravanan and Sivaraj [14] are compared through evaluating the Nusselt number and maximum strength of the streamlines for the different lengths of a rigid plate placed inside a square cavity as well as the different values of Rayleigh number. It is worth mentioning that for consistency, the average Nusselt numbers in Table 2 are measured on the outer cold wall, as was done by Saravanan and Sivaraj [14]. As shown in Table 2, the maximum difference between the present results and those achieved by Saravanan and Sivaraj [14] is 4.20%. Therefore, once again, the correctness and accuracy of the employed numerical approach and modeling is confirmed.

4. Results and discussion

In this section, the effects of different parameters on the flow and thermal fields and the flexible plate are investigated. These parameters are as follows: the Rayleigh number ($10^4 \le Ra \le 10^6$), the elasticity modulus ($5 \times 10^9 \le E_\tau \le 5 \times 10^{11}$), the Prandtl number (0.71, 6.2 and 200, representing air, water and a typical engine oil, respectively), the plate length ($0.1 \le l \le 0.7$) and the height of the plate from the origin ($-0.3 \le H \le 0.3$), while other parameters such as the non-dimensionless body force ($F_\nu = 0$), the thickness of the plate ($t_p = 0.01$) and the density ratio ($\rho_R = 1$) are kept constant during all simulations. Moreover, although the results show that variation of the dependent variables is diminished after about 0.2s, simulations are carried out for a larger time interval ($0.0 \le \tau \le 1.0$) to ensure the steady state condition.

Fig. 6 illustrates isothermal contours and streamlines of the fluid at different time steps until reaching the steady state condition. It can be found that two vortices appear in the streamlines at the early stages of the simulations, circulating in opposite directions near the vertical edges of the plate. At this time, conduction is the main mechanism of heat transfer, and the strength of the vortices are very low ($\tau < 5E\text{-}4$). As time elapses, the convection heat transfer plays a more significant role and therefore the strength of the vortices increase and impose the

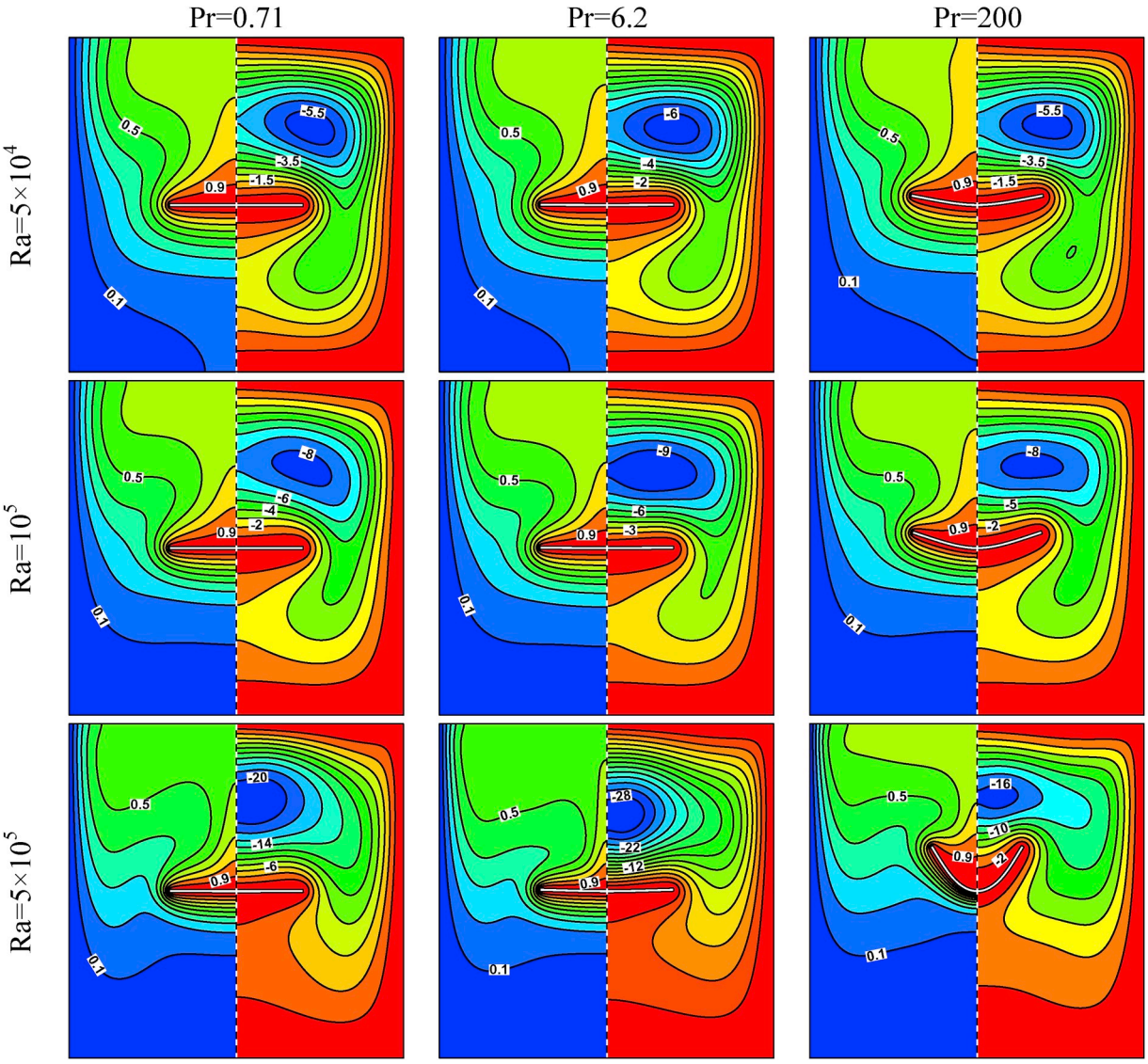

Fig. 8. Effect of Rayleigh and Prandtl numbers on the steady state Isotherms (left) and Streamlines (right) (H = 0.0, $E_\tau = 10^{11}$, l = 0.4).

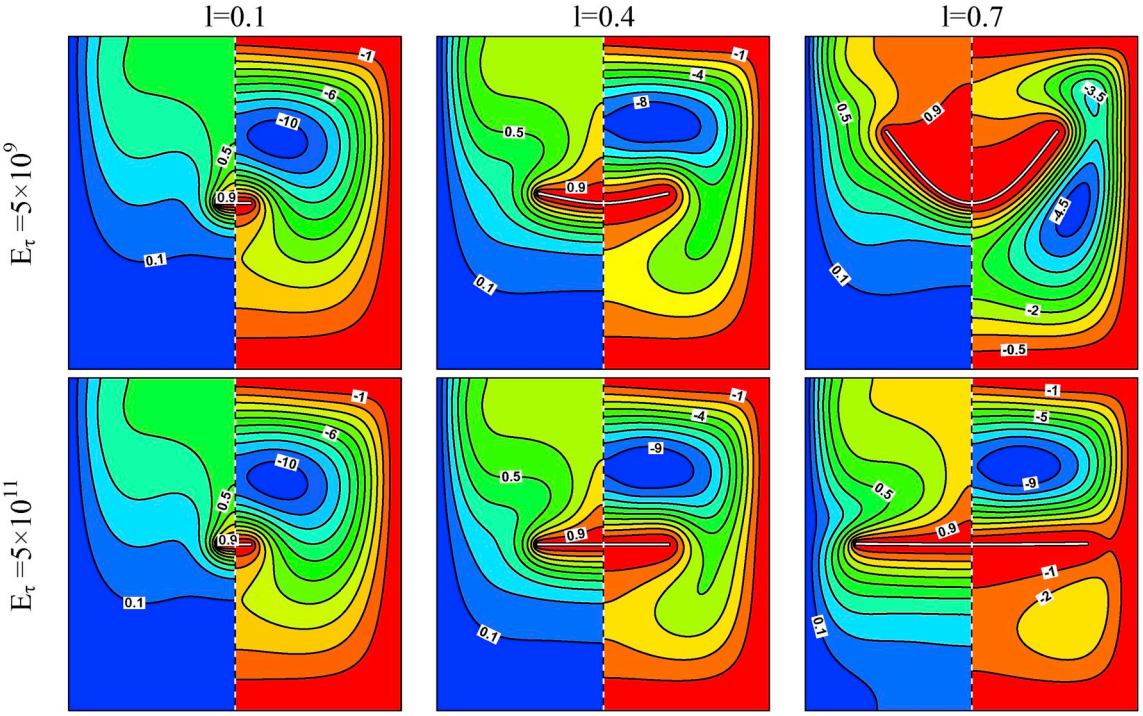

Fig. 9. Effect of the plate length and the elasticity modulus on the steady state Isotherms (left) and Streamlines (right) (Ra = 10^5, Pr = 6.2, H = 0.0).

required stress for the plate to bend. A new vortex appears and grows with the rate of deformation (5E-4 < τ < 5E-3) as the plate bends. However, at about τ = 7.5E-3, the new vortex is destroyed by the older vortices moving toward the upper space of the plate. The two separated vortices are finally merged to form a single stronger circulation above the deformed plate. As the plate deformation is directly related to the force exerted by the fluid motion, the plate exhibits different values of stress and strain before reaching the steady state condition.

Table 3 shows the variation of the flow rate and total heat transfer at different non-dimensional times and the elasticity modulus. By bending the plate, the average distance between hot and cold regions increases which causes a slight decrease in the overall rate of heat transfer. Thus, in comparison with the rigid plate case, the average Nusselt number on the hot plate is slightly lower. In addition to this, the fluid flow rate is again lower when compared to the rigid case. This happens because a portion of the fluid momentum is devoted to the plate deformation.

Fig. 7 depicts the effect of the Elasticity modulus E_τ and position of the plate H on the isotherms and streamlines of the fluid and the flexible plate, at the steady state condition. E_τ represents the resistance of the plate against the strain; therefore, the rate of deformation decreases as it increases. As mentioned before, the flow rate declines when the plate deformation increases. The isothermal lines move slightly toward the plate as the E_τ decreases, indicating a slight increment in the heat transfer rate.

On the other hand, the plate position shows a substantial impact on the isothermals and flow patterns which can be explained by lower effective space for the heat transfer, as the plate moves toward the top of the cavity. When the plate is near the top wall (H = 0.3), unlike other cases, two separate vortices appear beneath the plate, and the flow rate remains approximately unchanged with different values of the elasticity modulus. The rate of deformation shows that position of the plate can greatly influence the vortices strength and the rate of heat transfer.

The effect of the Rayleigh number Ra on the isotherms and streamlines of the fluid and the flexible plate at the steady state condition for different Prandtl numbers is shown in Fig. 8. It is clear that the Rayleigh number is a measure of buoyancy force; thus, increasing the Ra leads to an increase in the flow rate and consequently greater plate deformation. The isothermal lines move toward the plate by increasing the Rayleigh number, indicating an augment in the rate of heat transfer. Besides, it is seen that the increase of Prandtl number enhances the flow strength. This is due to that the momentum diffusion is higher than the heat diffusion when the Prandtl number is higher.

Fig. 9 illustrates the effect of the hot plate length on the flow and temperature fields of the cavity for two values of the elasticity modulus. It is clear that the length of the plate acts as a resistance against the buoyancy driven flow inside the cavity and thus reduces the strength of the streamlines. By increasing the hot plate length, the center of the vortices shifts toward below of the plate. Furthermore, increasing the

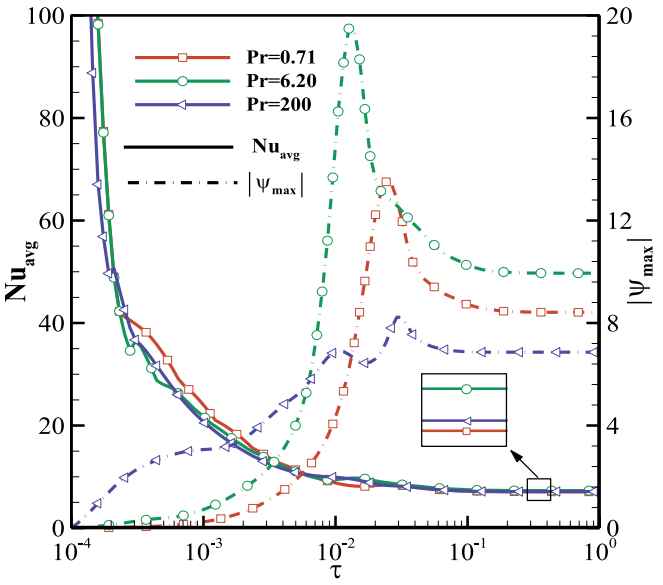

Fig. 10. Time variation of the average Nusselt number on the plate and the maximum value of the streamlines for different Prandtl numbers (H = 0.0, $E_\tau = 5\times10^{10}$, Ra = 10^5, l = 0.4).

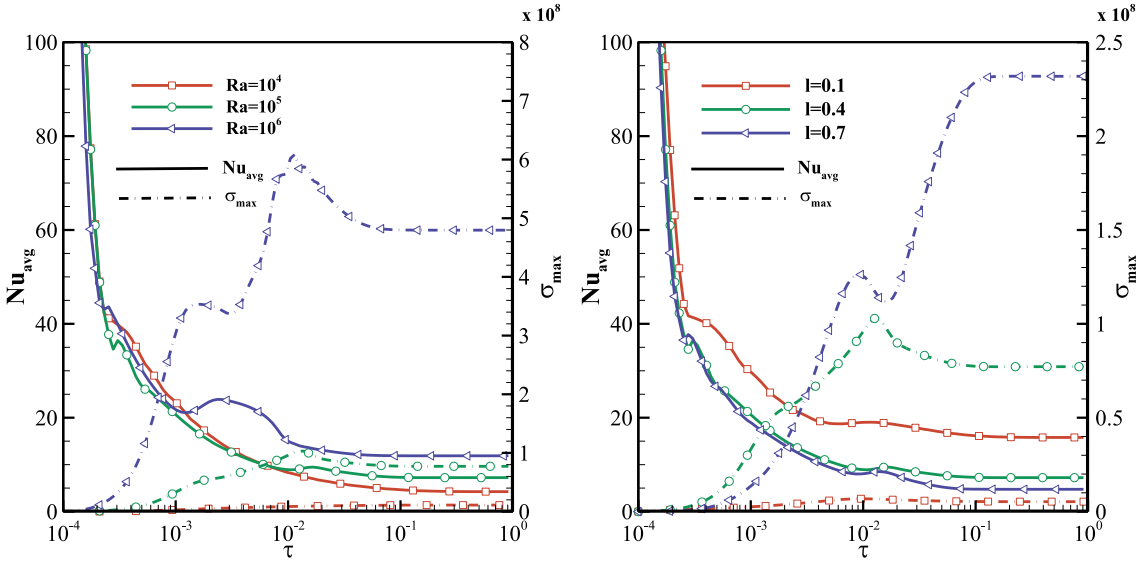

Fig. 11. Time variation of the average Nusselt number and the maximum value of the stress on the plate for different (left) Rayleigh numbers (H = 0.0, $E_\tau = 5 \times 10^9$, Pr = 6.2, l = 0.4) and (right) plate length (H = 0.0, Ra = 10^5, $E_\tau = 5 \times 10^9$, Pr = 6.2).

plate length divides the cavity into two separate regions when the deformation rate decreases ($E_\tau = 5 \times 10^{11}$ and $l = 0.7$) and the fluid is almost stagnant below the hot plate in this case. As a result, the heat is mainly transferred by conduction mechanism below the hot plate for the mentioned case, while the convection heat transfer dominates for the upper part. Moreover, there is a direct correlation between deformation and length of the plate as the exerted force on the hot plate enhances when its length increases (see the σ_{max} on Table 5 for different plate length).

Fig. 10 depicts the effect of the Prandtl numbers on the time variation of the average Nusselt number on the plate and the maximum of stream function. Elapsing time reduces the temperature difference between the hot plate and the fluid around it and therefore decreases the rate of heat transfer. Higher Prandtl number results in greater flow intensity and leads to the higher plate deformation, as shown in Fig. 8. Additionally, deformation of the plate reduces the fluid flow and increases the average distance between the hot and cold area and consequently reduces the average Nusselt number. Thus, as a result, and due to the plate deformation, the Nu_{avg} for water ($Pr = 6.2$) is greater than the others while for air ($Pr = 0.71$) and industrial oil ($Pr = 200$) are approximately equal. The maximum stream function increases as time passed, and reaches to its extrema at about $\tau \approx 0.1$–0.2 for air and water. For $Pr = 200$, due to the greater strain of the plate, the $|\psi_{max}|$ is lower even than $Pr = 0.71$. This is related to greater impact of the flow field on the plate. Moreover, shape of the $|\psi_{max}|$ for industrial oil is different in comparison with the other materials as discussed above.

Fig. 11 shows the effect of the Rayleigh number and the plate length on the time variation of the average Nusselt number and the maximum values of Von Mises stress on the plate. Increasing Ra leads to the greater Buoyancy force and therefore improves the rate of heat transfer. The behavior of the σ_{max} and Nu_{avg} at $Ra = 10^6$ is different with other values of Ra as this is related to the fact that at high Rayleigh numbers the plate exhibits different values of stresses and deformations. Increasing the plate length reduces the values of the average Nusselt number. This means that although the overall rate of heat transfer rises directly with the length of the plate, the rate of heat flux per surface area of the plate decreases as the hot plate length increases (Eq. (20)). Similar trend with the findings of Saravanan and Sivaraj [17] could be obtained if the average Nusselt number had been evaluated on the cold walls. As mentioned earlier, the exerted stress on the plate is raised as the length of the plate is increased.

Table 4 provides information about the effect of the plate position on the average Nusselt number for the both elastic and rigid case. It is evident that the plate position affects the rate of heat transfer strongly and the Nu_{avg} exhibits a drastic decrease as the plate position changes from the bottom of the cavity to its top, both for the flexible and rigid case. This is mainly due to the lower space and therefore weaker flow vortices which reduces the rate of heat transfer. Moreover, the reduction of the Nu_{avg} is more significant when the plate moves toward the top of the cavity, again for rigid and flexible plates. Although the plate deformation increases as the plate is placed near the bottom of the cavity (i.e. $H = -0.3$, see Fig. 7), the rate of heat transfer for the flexible plate is slightly higher than the rigid case. Since the average distance between the hot plate and cold walls is higher for the negative values of H, the plate deformation leads to the reduction of the mentioned distance and therefore enhance the average Nusselt number (for the case $H = -0.3$).

Influence of the Rayleigh and Prandtl numbers and the length of the plate on the flow and thermal fields of the fluid in the cavity are presented in Table 5. The first and second columns of the table represent the maximum values of stress on the plate in the steady-state condition ($\sigma_{max\text{-}SS}$) and the transient condition (σ_{max}), respectively. It can be found that for low flow rate of the fluid ($Ra = 10^4$), the stress (and therefore the plate deformation) reaches to its maximum value and remains unchanged before the steady state condition. While for the other simulation parameters, there is a quite large difference between the $\sigma_{max\text{-}SS}$ and σ_{max}, indicating that the plate deformation reduces after reaching its maximum value. Moreover, it is obvious that the flexibility reduces the rate of heat transfer and the flow rate. Furthermore, it should be noted that the effect of flexibility on the thermal and flow fields completely depends on the boundary conditions since it can improve or

Table 4
Impact of the plate position on the average Nusselt numbers and the maximum streamlines (Ra = 10^6, Pr = 6.2, Eτ = 5×10^{10}, l = 0.4).

H		−0.3	−0.15	0.0	0.15	0.3
Nu_{avg}	Flexible	12.647	12.527	12.071	11.218	8.8603
	Rigid	12.587	12.538	12.084	11.248	9.0217
$\lvert\psi_{max}\rvert$	Flexible	7.545	21.993	45.769	63.286	72.842
	Rigid	7.605	23.036	47.145	63.904	73.585

Table 5
Effect of the Ra, Pr and the plate length on the σ_{max} (in both transient and steady state), Nu_{avg} and $|\psi_{max}|$ (for the flexible and rigid plate) in the steady-state condition (H = 0.0).

		$\sigma_{max\text{-}SS}$	σ_{max}	Nu_{avg}	$Nu_{avg\text{-}Rigid}$	$\lvert\psi_{max}\rvert$	$\lvert\psi_{max\text{-}Rigid}\rvert$
Ra (E_τ = 5E9, Pr = 6.2, l = 0.4)	10^4	1.11E7	1.11E7 ($\tau \geq 0.155$)	4.2485	4.2546	1.774	1.8083
	10^5	7.72E7	1.03E8 ($\tau = 0.012$)	7.2346	7.3108	8.9669	10.043
	10^6	4.79E8	6.09E8 ($\tau = 0.011$)	11.882	12.084	26.318	47.145
Pr (Ra = 1E5, E_τ = 5E10, l = 0.4)	0.71	9.96E6	1.28E7 ($\tau = 0.020$)	7.0633	7.0645	8.418	8.433
	6.2	7.52E7	9.39E7 ($\tau = 0.010$)	7.3031	7.3108	9.939	10.040
	200	2.58E9	3.01E9 ($\tau = 0.026$)	7.1215	7.3407	6.862	10.084
l (Ra = 1E5, E_τ = 5E9, Pr = 6.2)	0.1	5.28E6	6.69E6 ($\tau = 0.013$)	15.792	15.792	10.621	10.626
	0.4	7.72E7	1.03E8 ($\tau = 0.012$)	7.2346	7.3108	8.9669	10.043
	0.7	2.32E8	2.32E8 ($\tau = 0.142$)	4.7516	5.6821	4.7951	10.014

reduce the rate of heat transfer (see Raisi and Arvin's work [24]). Finally, as discussed before, despite increasing the rate of heat transfer with raising the plate length, the average Nusselt number decreases, as it indicates the heat transferred rate per surface area of the hot plate.

5. Conclusion

In this study, the natural convection caused by a heated plate inside an enclosure was studied, and the effects of plate flexibility on the fluid flow and heat transfer were presented. It was assumed that the plate is at a higher temperature while the side walls of the cavity are cold and the bottom and top walls are insulated. Different ranges of modulus of elasticity, height and length of the plate, Rayleigh and Prandtl numbers on the fluid flow, Nusselt number, and stress were investigated. Some of the key findings of this research can be summarized as follow:

- The Nusselt number decreases as the flexibility increases, and also it increases as the plate moves toward the bottom of the cavity.
- The flow strength decreases as the plate becomes more flexible, while it increases as the plate moves toward the top of the enclosure.
- The Prandtl number has a negligible effect on the Nusselt number; however the Rayleigh number has greater effects on the Nusselt number.
- When the plate is rigid, the Nusselt number and flow strength increase with increasing the Prandtl number and Rayleigh number. However, for a flexible plate, Nusselt number and flow strength increase by changing the Prandtl number from 0.71 to 6.2 and then decrease by changing the Prandtl number from 6.2 to 200.
- Increasing the plate length reduces the rate of heat transfer per surface area of the plate.
- The steady state solution for the maximum stress on the plate shows that the stress increases with the Prandtl number, the plate length and the Rayleigh number.

References

[1] G. de Vahl Davis, Natural convection of air in a square cavity: a bench mark numerical solution, Int. J. Numer. Methods Fluids 3 (3) (1983) 249–264.
[2] N.C. Markatos, K.A. Pericleous, Laminar and turbulent natural convection in an enclosed cavity, Int. J. Heat Mass Transf. 27 (5) (1984) 755–772.
[3] H.F. Oztop, E. Abu-Nada, Numerical study of natural convection in partially heated rectangular enclosures filled with nanofluids, Int. J. Heat Fluid Flow 29 (5) (2008) 1326–1336.
[4] T. Fusegi, et al., A numerical study of three-dimensional natural convection in a differentially heated cubical enclosure, Int. J. Heat Mass Transf. 34 (6) (1991) 1543–1557.
[5] D. Cormack, L. Leal, J. Imberger, Natural convection in a shallow cavity with differentially heated end walls. Part 1. Asymptotic theory, J. Fluid Mech. 65 (2) (1974) 209–229.
[6] R.K.B. Gallegos, R.N. Sharma, Flags as vortex generators for heat transfer enhancement: gaps and challenges, Renew. Sustain. Energy Rev. 76 (2017) 950–962.
[7] A.K. Soti, R. Bhardwaj, J. Sheridan, Flow-induced deformation of a flexible thin structure as manifestation of heat transfer enhancement, Int. J. Heat Mass Transf. 84 (2015) 1070–1081.
[8] A. Al-Amiri, K. Khanafer, Fluid–structure interaction analysis of mixed convection heat transfer in a lid-driven cavity with a flexible bottom wall, Int. J. Heat Mass Transf. 54 (17) (2011) 3826–3836.
[9] K. Khanafer, Fluid–structure interaction analysis of non-Darcian effects on natural convection in a porous enclosure, Int. J. Heat Mass Transf. 58 (1) (2013) 382–394.
[10] E. Jamesahar, M. Ghalambaz, A.J. Chamkha, Fluid–solid interaction in natural convection heat transfer in a square cavity with a perfectly thermal-conductive flexible diagonal partition, Int. J. Heat Mass Transf. 100 (2016) 303–319.
[11] M. Ghalambaz, et al., Fluid-structure interaction study of natural convection heat transfer over a flexible oscillating fin in a square cavity, Int. J. Therm. Sci. 111 (2017) 256–273.
[12] S. Mehryan, et al., Analysis of fluid-solid interaction in MHD natural convection in a square cavity equally partitioned by a vertical flexible membrane, J. Magn. Magn. Mater. 424 (2017) 161–173.
[13] S.A.M. Mehryan, et al., Fluid–structure interaction analysis of free convection in an inclined square cavity partitioned by a flexible impermeable membrane with sinusoidal temperature heating, Meccanica 52 (11) (2017) 2685–2703.
[14] A.K. Abdul Hakeem, S. Saravanan, P. Kandaswamy, Natural convection in a square cavity due to thermally active plates for different boundary conditions, Comput. Math. Appl. 62 (1) (2011) 491–496.
[15] S. Saravanan, C. Sivaraj, Coupled thermal radiation and natural convection heat transfer in a cavity with a heated plate inside, Int. J. Heat Fluid Flow 40 (2013) 54–64.
[16] L. Boukhattem, H. Hamdi, D.R. Rousse, Numerical simulation of heat transfers in a room in the presence of a thin horizontal heated plate, Energy Procedia 42 (2013) 549–556.
[17] S. Saravanan, C. Sivaraj, Combined natural convection and thermal radiation in a square cavity with a nonuniformly heated plate, Comput. Fluids 117 (2015) 125–138.
[18] W. Zhang, et al., Partitioning effect on natural convection in a circular enclosure with an asymmetrically placed inclined plate, Int. Commun. Heat Mass Transf. 90 (2018) 11–22.
[19] S.A.M. Mehryan, et al., Mixed convection flow caused by an oscillating cylinder in a square cavity filled with Cu–Al2O3/water hybrid nanofluid, J. Therm. Anal. Calorim. 137 (3) (2019) 965–982.
[20] The finite element method for fluid dynamics, in: O.C. Zienkiewicz, R.L. Taylor, P. Nithiarasu (Eds.), The Finite Element Method for Fluid Dynamics, seventh ed., Butterworth-Heinemann, Oxford, 2014, p. iii.
[21] U. Küttler, W.A. Wall, Fixed-point fluid–structure interaction solvers with dynamic relaxation, Comput. Mech. 43 (1) (2008) 61–72.
[22] F. Xu, J.C. Patterson, C. Lei, Heat transfer through coupled thermal boundary layers induced by a suddenly generated temperature difference, Int. J. Heat Mass Transf. 52 (21) (2009) 4966–4975.
[23] B. Calcagni, F. Marsili, M. Paroncini, Natural convective heat transfer in square enclosures heated from below, Appl. Therm. Eng. 25 (16) (2005) 2522–2531.
[24] A. Raisi, I. Arvin, A numerical study of the effect of fluid-structure interaction on transient natural convection in an air-filled square cavity, Int. J. Therm. Sci. 128 (2018) 1–14.